JOURNAL OF PROPULSION AND POWER
Vol. 23, No. 1, January–Febrary 2007

Technical Notes

TECHNICAL NOTES are short manuscripts describing new developments or important results of a preliminary nature. These Notes should not exceed 2500 words (where a figure or table counts as 200 words). Following informal review by the Editors, they may be published within a few months of the date of receipt. Style requirements are the same as for regular contributions (see inside back cover).

Quadrant Analysis of a Mixer–Ejector Nozzle for Supersonic Transport Applications

Dennis A. Yoder,* Nicholas J. Georgiadis,† and John D. Wolter†
NASA John H. Glenn Research Center at Lewis Field, Cleveland, Ohio 44135

DOI: 10.2514/1.25258

Nomenclature

C_{fg}	=	gross thrust coefficient, $F_g/\dot{m}_p V_{p_{\text{ideal}}}$
F_g	=	gross thrust
k	=	turbulence kinetic energy
L	=	mixing duct length
$\dot{m}_p$	=	primary mass flow rate
$\dot{m}_s$	=	secondary mass flow rate
$V_{p_{\text{ideal}}}$	=	ideal (perfectly expanded) primary jet velocity
x	=	axial distance from mixer exit plane
y	=	spanwise distance from center of mixing duct
z	=	vertical distance from center of mixing duct
ϵ	=	turbulent dissipation rate
γ	=	ratio of specific heats
ω	=	pumping ratio, $\dot{m}_s/\dot{m}_p$

Introduction

A decade ago, NASA's High Speed Research (HSR) program was actively developing enabling technologies for a 300 passenger supersonic commercial transport that would supersede the Concorde and reduce transoceanic travel times by a factor of 2 relative to subsonic transports. Even though the program ended in 1999, much of the technical information generated has only recently been made available for public dissemination. The purpose of this note is to describe the results from one study of this larger effort to develop a mixer–ejector nozzle.

One of the key technological challenges of any next-generation supersonic transport is the requirement to meet stringent community noise regulations, which are particularly restrictive at the takeoff condition where maximum engine thrust is necessary. The primary component of aircraft noise during takeoff is jet noise produced by the interaction of the turbulent nozzle exhaust flow with the ambient air.

One concept for reducing jet exhaust noise studied extensively in this program was the lobed mixer–ejector nozzle shown in Fig. 1. References [1–3] describe the basic principles of these flow devices. Hot flow from the turbine exhaust leaves the primary side of the ejector array and overexpands, creating a pressure gradient that entrains additional freestream air through the secondary inlet. The lobed shape of the ejector array enhances the mixing between streams by 1) generating large-scale streamwise vortices and/or 2) increasing the perimeter of the shear layer between the primary and secondary streams. After passing through a mixing duct, the combined flow has a lower nozzle exit velocity and, consequently, produces lower noise levels. However, the entrainment of secondary air enhances the mass flow rate such that the resultant thrust remains acceptably high. At cruise, the secondary inlet is closed to allow optimum performance of the nozzle.

Experimental testing of these mixer–ejector nozzle concepts is difficult and expensive, particularly because both performance and acoustic data are needed for evaluation. Computational fluid dynamics (CFD) was used to perform preliminary analyses to identify the relative performance of different nozzle concepts. This information was used to down-select concepts for testing in one of the experimental facilities. In particular, CFD was used to perform chute-shaping studies and evaluate the effect of lobe count.

At the time, however, CFD was only beginning to be applied to complex geometric configurations on a routine basis. Limitations in grid generation software and computational hardware severely restricted the turnaround time for such calculations. For example, the configuration shown in Fig. 1 has two planes of symmetry that allow one to predict the performance of the nozzle by modeling just one quadrant of the overall geometry in a Reynolds-averaged Navier–Stokes calculation. However, due to the large number of grid points needed to accurately resolve a complete quadrant of the lobed mixer–ejector nozzle and the complexity of the grid generation task, most of the trade studies used to evaluate the effect of various chute shape parameters were conducted assuming periodicity in the spanwise direction. This assumption reduced the necessary computational domain to just one half-wavelength of the ejector geometry that extended from the peak of one primary flow chute to the trough of the nearest secondary flow chute. Although this approach is more computationally efficient, any effects due to the sidewalls are absent.

Because the ejector geometry contained a number of lobes in the spanwise direction, it was thought that these sidewall effects would remain localized to the near-wall region. However, experimental measurements [4] indicated the presence of a significant region of unmixed flow along the sidewall near the *xy*-symmetry plane. The objective of the study presented in this note was to investigate the effect of the sidewall on the flow within the mixing duct and attempt to explain the formation of this unmixed region. Results obtained from a half-chute simulation are compared with those from a quadrant simulation and available experimental data to ascertain the validity of the symmetry assumption away from the sidewall and to determine how much of an impact the sidewall had on the performance parameters.

Geometry and Flow Conditions

The particular mixer–ejector nozzle under examination is the downstream mixer (DSM), which was tested [4] at the Boeing Low Speed Aeroacoustic Facility. This geometry is referred to as an axial mixer rather than a vortical mixer, because the mixer lobes are designed to direct the primary and secondary streams in the axial direction and rely upon the increased perimeter of the shear layer

Received 18 May 2006; accepted for publication 16 July 2006.

*Aerospace Engineer, Inlet and Nozzle Branch. Senior Member AIAA.
†Aerospace Engineer, Inlet and Nozzle Branch. Associate Fellow AIAA.

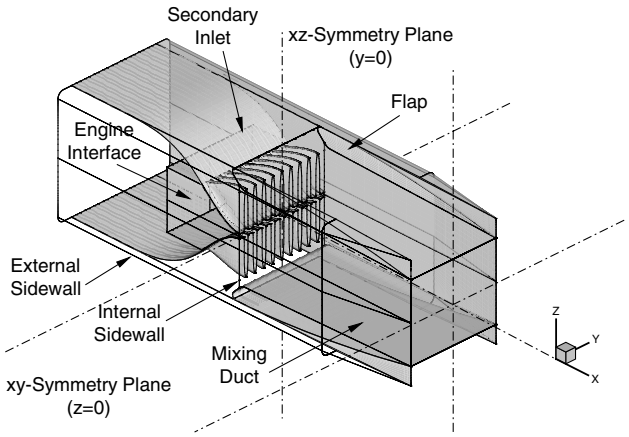

Fig. 1 Schematic of downstream mixer (DSM) nozzle.

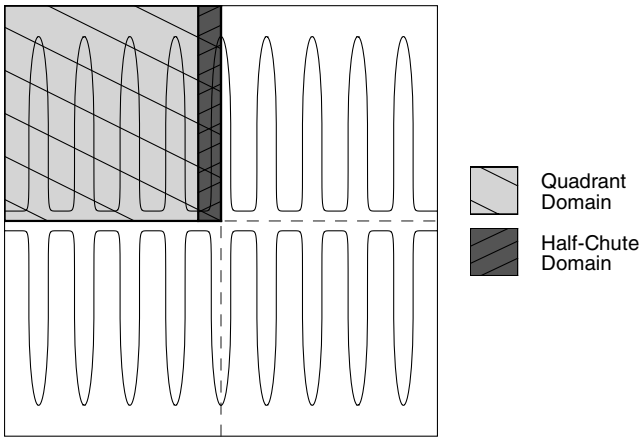

Fig. 2 Comparison of internal flow computational domains for quadrant and half-chute calculations.

rather than the vortical nature of the flow to achieve efficient mixing. As shown in Fig. 1, both the top and bottom mixer–chute arrays contain nine primary and ten secondary chutes across the width of the nozzle. The secondary chute nearest the sidewall extends roughly one additional half-chute width in the spanwise direction. This type of chute design, referred to as a full-cold chute along the sidewall, was designed to entrain additional secondary mass flow and reduce thermal stresses on the sidewalls. For this particular configuration, the base region of the primary chute also extends to the sidewall. A detailed description of the geometric parameters is given in [4], and the results presented herein correspond to configuration 953.576 from the experimental test matrix.

The flow conditions simulated were as follows: the total temperature of the primary nozzle flow was 1551 deg Rankine and the nozzle was operated at a primary nozzle pressure ratio of 3.43. The freestream stagnation pressure and temperature were prescribed, corresponding to a freestream Mach number of 0.07. Whereas the experimental data were obtained statically, the CFD analysis required this small freestream flow to enhance the stability and convergence rate of the code. Similar difficulties have been encountered in related studies [5] when trying to simulate such flows with a compressible flow solver. Although the use of this slow freestream flow may cause a very slight increase in the observed pumping ratio, it does not significantly alter the flow development within the secondary inlet and mixing duct. The reason is that the flow entrainment is driven by the ratio of the freestream stagnation pressure to the effective static pressure that the secondary stream sees at the end of the mixer chutes inside the ejector. Changing the freestream Mach number to 0.07 only increases the freestream stagnation pressure by 0.34%.

Experimental data are available for the pumping ratio (the ratio of secondary to primary mass flow rates) and gross thrust. Surveys of the axial velocity and total temperature were also measured within one quadrant of the duct exit plane using a five hole probe. For the results presented here, the data have been reflected to the other quadrants to provide contours over the entire duct exit area.

Computational Domain

In this study, the quadrant simulation was conducted in the $(\pm x, -y, +z)$ region of the schematic shown in Fig. 1. The computational domain includes all of the hardwall surfaces shown (the lobed mixer chutes, the internal sidewall along the primary and secondary flow passages and the mixing duct, as well as the freestream flow over the external shroud surface and flap). These surfaces were treated as adiabatic viscous walls. The inflow boundary for the primary nozzle was placed upstream of the ejector array where the primary nozzle interfaces with the engine, and uniform values for total temperature and pressure were specified. Freestream conditions were specified for flow external to the nozzle, and the outflow boundary was placed approximately five duct heights downstream of the duct exit plane.

For the half-chute calculation, the computational domain consisted of the half-chute region nearest the xz symmetry plane ($y = 0$). As illustrated in Fig. 2, this region extends from the peak of the center primary chute to the trough of the adjacent secondary chute. An additional symmetry condition was imposed along the xz plane that runs through the trough of the secondary chute. None of the other chutes, the internal sidewall, or the external shroud surface were modeled. Freestream flow through the secondary inlet and over the external flap surface was included in these calculations.

In the results to be presented, the half-chute solutions were reflected and copied several times in the spanwise direction to enable a more direct comparison with the quadrant solutions. Contours at the duct exit plane are presented over the entire width and height of the mixing duct. These were generated by further reflecting the solutions to fill the other quadrants of the duct.

Computational Mesh

Table 1 lists the distribution of grid points for each of the major flow regions within the half-chute and quadrant domains. The computational mesh for the primary and secondary flow region on either side of each of the mixer lobes was constructed using two point-matched grid blocks. The first block was used to represent the base region, for example, the primary flow region near the $z = 0$ plane, whereas the second block extended in the z direction to represent the chute region. This technique significantly reduces the skewness of the grid compared with other topologies while still enabling one to efficiently cluster points toward the lobe surface. These blocks interfaced with a rectangular mesh defining the mixing duct region, which was clustering near the mixer exit plane to resolve the shear layer between the primary and secondary streams. A single rectangular grid was used to model the entire plume region.

As shown in Table 1, the total number of grid points used in the quadrant calculations is more than an order of magnitude greater than that used in the half-chute simulation. Although the 4×10^6 points used in the quadrant simulation may not seem unreasonable by today's standards, at the time this work was conducted this represented a significant computational effort that required several months to complete on a multiprocessor machine. Because of this, an exhaustive grid sensitivity analysis was not conducted for these

Table 1 Distribution of grid points within the computational domain

Flow domain	Half-chute	Quadrant
Primary flow	38,658	359,346
Secondary flow	78,324	804,690
Mixing duct	178,266	1,734,042
External flow	56,010	617,232
External sidewall flow	0	128,520
Plume	31,977	428,868
Total	383,235	4,072,698

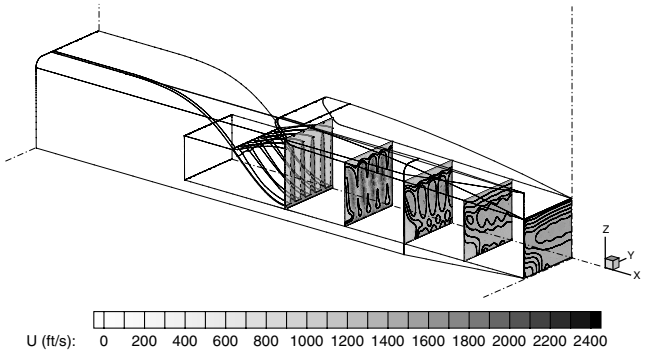

Fig. 3 Axial velocity contours of quadrant solution inside mixing duct.

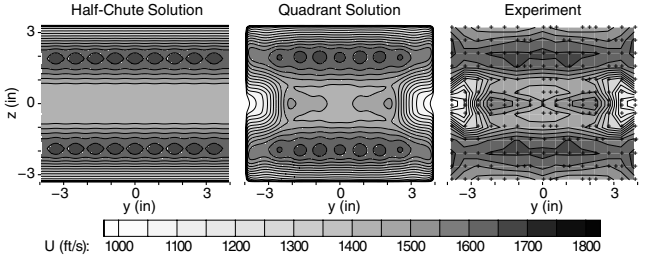

Fig. 4 Axial velocity contours at duct exit plane.

nozzle calculations. However, the grid topology and density for the half-chute and quadrant simulations were selected based upon previous analysis performed by the multiorganizational HSR CFD analysis team [6].

Computational Algorithm

Calculations were performed using the NPARC finite difference code [7,8], which solves the conservation law form of the Reynolds-averaged Navier–Stokes equations. Steady-state solutions were obtained with an approximate factorization algorithm and second order accurate central differencing for the spatial derivatives. Default settings for the artificial dissipation were used to keep the algorithm stable. Turbulence was modeled using the low-Reynolds number two-equation k–ϵ model of Chien [9], but consistent with the recommendations of [6] no corrections for compressibility or vortex stretching were included for these calculations. The flow was assumed to behave as a perfect gas with $\gamma = 1.4$.

Convergence criteria for these cases included monitoring of the residual error as well as integral flow quantities such as mass flow rates through the mixing duct, thrust coefficients, and pumping ratio. Solutions were determined to have reached steady state once a three-order reduction in residual had been achieved and the mass flow rate through the mixing duct was conserved within 0.5%. The resultant values for the pumping ratio and gross thrust coefficient were converged within 0.2% and 0.3%, respectively.

Table 2 Nozzle performance results

Parameter	Half-chute	Quadrant	Experiment
ω	0.531	0.556	0.545
C_{fg}	0.990	0.981	0.980

Results

Figure 3 presents the quadrant results for the axial velocity contours inside the mixing duct. These contours show how the mixing process acts to merge the initially segregated primary and secondary flows leaving the ejector chutes. Along the sidewall, beginning at the $x/L = 0.25$ location, a region of low velocity flow is observed that persists to the nozzle exit.

Axial velocity contours at the nozzle exit plane are compared with the half-chute results and experimental data in Fig. 4. The size and shape of the low velocity region are well predicted by the quadrant solution. The three-dimensional effects due to the sidewall are not limited to the near-wall region, but instead appear to extend nearly half the distance from the sidewall to the center plane. The half-chute solution is therefore representative of the nozzle flowfield only across half of the nozzle span.

Total temperature contours within the mixing duct and at the nozzle exit were also examined and found to exhibit many of the same characteristics as the velocity contours of Figs. 3 and 4. In the interest of space these results are not included here, but may be found in [10].

Table 2 compares the computed pumping and thrust with experimental data. Values listed for the half-chute solutions were determined using only the half-chute domain on which the CFD was computed and do not include any corrections for the additional entrained mass flow near the sidewall. Therefore, one would expect the quadrant solution to yield greater pumping than the half-chute solution, and in fact this holds true. Comparison with the experimental data indicates that the quadrant solution overpredicts the pumping ratio (ω) by 2.0%, whereas the half-chute solution underpredicts the pumping ratio by roughly 2.5%. The gross thrust coefficient (C_{fg}) of the quadrant solution compares very favorably with the experimental data. The half-chute solution, which does not account for the sidewall losses, is found to overpredict the thrust by 1.0%.

Further examination of the quadrant solution was undertaken to better understand the source of the low-energy flow regions along the sidewalls. It was originally speculated that, as the freestream spilled over the external sidewall and into the secondary inlet, it rolled into a vortex. This vortex was then thought to pass through the bottom of the secondary chute nearest the sidewall and along the length of the mixing duct. Examination of the streamlines in Fig. 5 indicates that a

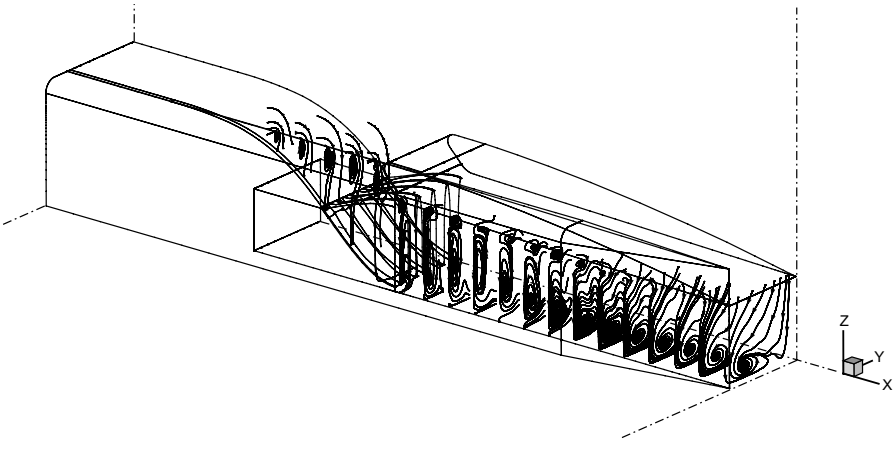

Fig. 5 Cross-flow stream lines within the mixer–ejector nozzle.

vortex is formed from the corner of the secondary inlet. However, it does not convect through the bottom of the secondary chute. At the chute exit plane, this vortex is instead observed just above the peak of the primary chute in the corner formed by the flap and sidewall. Inside the mixing duct, this vortex interacts with the primary flow from the chute nearest the sidewall, drawing it away from the $z = 0$ symmetry plane and pushing the secondary flow near the sidewall in the opposite direction. This is somewhat evident in the axial velocity contours of Fig. 3 at the $x/L = 0.25$ location. The low-energy region observed at the duct exit plane is therefore not the remnant of a vortex core generated by the secondary inlet, but is instead an artifact of the interaction of that upstream vortex with the primary flow.

With this understanding of how the sidewall flow evolves, recommendations can be made for altering the nozzle design to obtain a more fully mixed flow at the duct exit. One possibility would be to modify the secondary inlet to prevent the formation of the vortex or to add flow control devices to help dissipate the vortex before it enters the mixing duct. Another possibility, and the one pursued in the HSR program, would be to reduce or eliminate the secondary chute nearest the sidewall. The size of the low-energy region appears be linked to the full-cold chute near the sidewalls. Reducing the size of this chute would limit the amount of secondary flow that can be forced toward the $z = 0$ symmetry plane. However, this choice requires that the mixer lobes be redesigned and rescaled to maintain the necessary area ratios, pumping ratio, and thrust. In addition, the sidewalls must be redesigned to handle the elevated wall temperatures.

Conclusions

In this study, computational fluid dynamics was used to investigate the effect of the sidewall on flow within the mixing duct downstream of a lobed mixer–ejector nozzle. Solutions obtained from half-chute and full-quadrant simulations of the nozzle confirm that away from the sidewall the half-chute symmetry assumption appears to be valid. However, there is a significant region of low-energy flow along the sidewall that can only be predicted by a quadrant simulation. This nonuniform flow at the mixing duct exit plane was found not to be the remnant of a vortex fed through the secondary inlet, but instead is the result of that vortex interacting with the hot primary flow inside the mixing duct. Understanding of this phenomenon led to recommended modifications to the nozzle design.

References

[1] Stern, A., and Peracchio, A., "The Challenge of Reducing Supersonic Civil Transport Noise," AIAA Paper 89-2363, July 1989.

[2] Lord, W. K., Jones, C. W., Stern, A. M., Head, V. L., and Krejsa, E. A., "Mixer Ejector Nozzle for Jet Noise Suppression," AIAA Paper 90-1909, July 1990.

[3] Bevilaqua, P. M., "Advances in Ejector Thrust Augmentation," SAE Paper 872322, 1988.

[4] Arney, L., Sandquist, D., Forsyth, D., and Lidstone, G., "Gen 2.0 Mixer/Ejector Nozzle Test at Boeing Low Speed Aeroacoustic Facility June 1995–July 1996," NASA CR-2005-213334, Feb. 2005.

[5] Barber, T., Chiappetta, L., and Zysman, S. H., "Assessment of Jet Noise Analysis Codes for Multistream Axisymmetric and Forced Mixer Nozzles," *Journal of Propulsion and Power*, Vol. 13, No. 6, 1997, pp. 737–744.

[6] Barber, T., Chiappetta, L., Debonis, J., Georgiadis, N., and Yoder, D., "Assessment of Parameters Influencing the Prediction of Shear-Layer Mixing," *Journal of Propulsion and Power*, Vol. 15, No. 1, 1999, pp. 45–53.

[7] Cooper, G., and Sirbaugh, J., "The PARC Distinction: A Practical Flow Simulator," AIAA Paper 90-2002, July 1990.

[8] Power, G. D., Cooper, G. K., and Sirbaugh, J. R., "NPARC 2.2–Features and Capabilities," AIAA Paper 95-2609, July 1995.

[9] Chien, K.-Y., "Predictions of Channel and Boundary-Layer Flows with a Low Reynolds Number Turbulence Model," *AIAA Journal*, Vol. 20, No. 1, 1982, pp. 33–38.

[10] Yoder, D. A., Georgiadis, N. J., and Wolter, J. D., "Quadrant CFD Analysis of a Mixer-Ejector Nozzle for HSCT Applications," NASA TM-2005-213602, April 2005.

F. Liu
Associate Editor